AGU PUBLICATIONS

JGR

Journal of Geophysical Research: Atmospheres

RESEARCH ARTICLE
10.1002/2014JD021888

Key Points:
- ATOFMS field data used for the first time to predict hygroscopicity
- Predictions agree well with measurements
- External mixing of aerosol can be determined

Supporting Information:
- Readme
- Figure S1
- Figure S2
- Figure S3
- Figure S4
- Figure S5
- Figure S6
- Figure S7
- Figure S8
- Figure S9
- Figure S10
- Figure S11
- Figure S12
- Figure S13
- Figure S14
- Figure S15
- Figure S16
- Figure S17

Correspondence to:
R. M. Healy,
robert.healy@utoronto.ca

Citation:
Healy, R. M., et al. (2014), Predicting hygroscopic growth using single particle chemical composition estimates, *J. Geophys. Res. Atmos.*, *119*, 9567–9577, doi:10.1002/2014JD021888.

Received 9 APR 2014
Accepted 21 JUL 2014
Accepted article online 24 JUL 2014
Published online 4 AUG 2014

Predicting hygroscopic growth using single particle chemical composition estimates

Robert M. Healy[1,2], Greg J. Evans[1], Michael Murphy[1], Zsófia Jurányi[3,4], Torsten Tritscher[3,5], Marie Laborde[3,6], Ernest Weingartner[3,4], Martin Gysel[3], Laurent Poulain[7], Katharina A. Kamilli[7,8], Alfred Wiedensohler[7], Ian P. O'Connor[2], Eoin McGillicuddy[2], John R. Sodeau[2], and John C. Wenger[2]

[1]Southern Ontario Centre for Atmospheric Aerosol Research, University of Toronto, Toronto, Ontario, Canada, [2]Department of Chemistry and Environmental Research Institute, University College Cork, Cork, Ireland, [3]Laboratory of Atmospheric Chemistry, Paul Scherrer Institute, Villigen, Switzerland, [4]Now at Institute of Aerosol and Sensor Technology, University of Applied Sciences, Windisch, Switzerland, [5]Now at TSI GmbH, Aachen, Germany, [6]Now at Ecotech Pty Ltd., Knoxfield, Australia, [7]Leibniz Institute for Tropospheric Research, Leipzig, Germany, [8]Now at University of Bayreuth, Bayreuth Center of Ecology and Environmental Research, Bayreuth, Germany

Abstract Single particle mass spectral data, collected in Paris, France, have been used to predict hygroscopic growth at the single particle level. The mass fractions of black carbon, organic aerosol, ammonium, nitrate, and sulphate present in each particle were estimated using a combination of single particle mass spectrometer and bulk aerosol chemical composition measurements. The Zdanovskii-Stokes-Robinson (ZSR) approach was then applied to predict hygroscopic growth factors based on these mass fraction estimates. Smaller particles with high black carbon mass fractions and low inorganic ion mass fractions exhibited the lowest predicted growth factors, while larger particles with high inorganic ion mass fractions exhibited the highest growth factors. Growth factors were calculated for subsaturated relative humidity (90%) to enable comparison with hygroscopic tandem differential mobility analyzer measurements. Mean predicted and measured hygroscopic growth factors for 110, 165, and 265 nm particles were found to agree within 6%. Single particle-based ZSR hygroscopicity estimates offer an advantage over bulk aerosol composition-based hygroscopicity estimates by providing additional chemical mixing state information. External mixing can be determined for particles of a given diameter through examination of the predicted hygroscopic growth factor distributions. Using this approach, 110 nm and 265 nm particles were found to be predominantly internally mixed; however, external mixing of 165 nm particles was observed periodically when thinly coated and thickly coated black carbon particles were simultaneously detected. Single particle-resolved chemical information will be useful for modeling efforts aimed at constraining cloud condensation nuclei activity and hygroscopic growth.

1. Introduction

Single particle mass spectrometer data have proven to be useful for the association of climate-relevant properties including hygroscopicity and ice nucleation activity with different aerosol internal mixtures [*Buzorius et al.*, 2002; *Cziczo et al.*, 2006; *Herich et al.*, 2008, 2009; *Zelenyuk et al.*, 2010; *Corbin et al.*, 2012; *Cziczo et al.*, 2013; *Hersey et al.*, 2013]. However, it is challenging to use the chemical information provided by single particle mass spectrometers quantitatively [*Allen et al.*, 2006; *Qin et al.*, 2006; *Sullivan et al.*, 2009; *Healy et al.*, 2013], and this has precluded the calculation of composition-based hygroscopicity estimates at the single particle level. Conversely, bulk aerosol chemical composition data are often used to directly predict hygroscopic growth for ambient particle ensembles using the Zdanovskii-Stokes-Robinson (ZSR) mixing rule [*Svenningsson et al.*, 2006; *Gysel et al.*, 2007; *Hegg et al.*, 2008; *Sjogren et al.*, 2008; *Kamilli et al.*, 2014; *Levin et al.*, 2014], and size-resolved aerosol mass spectrometer measurements of nonrefractory bulk aerosol have been used to predict size-resolved particle hygroscopicity [*Gysel et al.*, 2007; *Hersey et al.*, 2009; *Wu et al.*, 2013]. More recently, soot particle aerosol mass spectrometers (SP-AMS) have enabled simultaneous size-resolved measurement of bulk refractory black carbon (BC) and nonrefractory aerosol, leading to an improvement in composition-based hygroscopicity predictions [*Liu et al.*, 2013]. However, aerosol mass spectrometers measure particle ensembles and therefore do not provide explicit chemical mixing state information.

In order to predict the effect of changes in composition and mixing state upon particle hygroscopicity, chemical composition data at the single particle level are desirable. This information is expected to be

©2014. American Geophysical Union. All Rights Reserved.

particularly useful for climate models aimed at improving the accuracy of aerosol microphysical properties by incorporating mixing state [*Riemer et al*., 2009; *Bauer et al*., 2013]. Knowledge of single particle composition for particles of a given diameter would enable predictions of multimodal hygroscopic growth factor distributions in environments where external mixing is relevant. Although laser desorption/ionization-based single particle mass spectrometer measurements are subject to detection efficiency issues associated predominantly with composition-dependent matrix effects, recent quantitative estimates of single particle composition have been derived for a range of refractory and nonrefractory chemical species [*Ferge et al*., 2006; *Pratt et al*., 2009; *Froyd et al*., 2010; *Jeong et al*., 2011; *Healy et al*., 2013].

A substantial fraction of BC particles in Paris, France, during the winter months have been previously demonstrated to be externally mixed using single particle soot photometer (SP2) measurements [*Laborde et al*., 2013]. This external mixing impacts the likelihood that these particles will act as cloud condensation nuclei. The aim of this work is to predict hygroscopic growth at the single particle level for the same period based on single particle chemical composition information. A combination of single particle mass spectrometer, aerosol mass spectrometer, and multiangle absorption photometer data is used to estimate single particle mass and volume fractions for BC, organic aerosol (OA), ammonium, nitrate, and sulphate. The ZSR mixing rule is then applied to predict hygroscopic growth (for relative humidity = 90%) based on the estimated volume fraction of each species present in each particle. Predicted hygroscopic growth data are compared with simultaneous hygroscopic tandem differential mobility analyzer (HTDMA) measurements collected at a separate sampling site located 20 km away. The results obtained from this new approach are also discussed in the context of the previous SP2 findings.

2. Methods

2.1. Sampling Sites and Instrumentation

2.1.1. Laboratoire d'Hygiène de la Ville de Paris Site

The Laboratoire d'Hygiène de la Ville de Paris (LHVP) site is located in central Paris (48.75°N, 2.36°E) and measurements were performed from 15 January 2010 to 11 February 2010. All measurements described here were performed as part of the MEGAPOLI (Megacities: Emissions, urban, regional and Global Atmospheric POLlution and climate effects, and Integrated tools for assessment and mitigation) campaign. The instruments used for the measurement of aerosol chemical composition at the LHVP site have been described in detail elsewhere [*Healy et al*., 2013]. Briefly, an aerosol time-of-flight mass spectrometer (ATOFMS, TSI) [*Gard et al*., 1997] fitted with an aerodynamic lens (AFL100, TSI) [*Su et al*., 2004] was used to collect size-resolved single particle mass spectral data. Particles are sampled through a critical orifice, focused in the aerodynamic lens, and their velocity, measured as the time-of-flight between two sizing lasers (Nd:YAG, 532 nm), is used to calculate their corresponding vacuum aerodynamic diameter (d_{va}). Sizing efficiency is dependent upon particle diameter, with lower efficiencies observed for particles of decreasing size in the range 100–500 nm [*Su et al*., 2004; *Healy et al*., 2012]. The particle velocity is also used to estimate arrival time in the mass spectrometry region of the instrument, where a Q-switched UV laser (Nd:YAG, 266 nm) desorbs and ionizes particle components. The ions formed are detected using a dual ion time-of-flight mass spectrometer. Positive and negative ion mass spectra are thus collected for each single particle successfully ionized. A multiangle absorption photometer (MAAP, 5012, Thermo) [*Petzold and Schönlinner*, 2004] and a high-resolution time-of-flight aerosol mass spectrometer (HR-ToF-AMS, Aerodyne) [*DeCarlo et al*., 2006] were also deployed at the LHVP site. A collection efficiency of 0.4 was calculated for the HR-ToF-AMS as discussed elsewhere [*Crippa et al*., 2013]. The HR-ToF-AMS and MAAP sampled aerosol at 6 m above ground level through a PM_{10} inlet fitted with an aerosol diffusion dryer [*Tuch et al*., 2009]. The ATOFMS sampled aerosol through a separate stainless steel inlet at 4 m above ground level. Although aerosol was not dried prior to sampling for the ATOFMS inlet, the use of an aerodynamic lens system has been demonstrated previously to minimize particle water content prior to sizing and detection [*Zelenyuk et al*., 2006]. Particles with high water content are typically characterized by poor negative ion formation and detection in the dual ion mass spectrometer [*Neubauer et al*., 1998], an effect that was not observed for this data set even during a fog event on 18 January 2010 [*Healy et al*., 2012]. It would be prudent in future studies, however, to dry the aerosol prior to detection for all instruments involved, to minimize any potential artifacts associated with particle phase water.

2.1.2. Site Instrumental de Recherche par Télédétection Atmosphérique Site

The SIRTA (Site Instrumental de Recherche par Télédétection Atmosphérique) site is located on the outskirts of Paris, approximately 20 km southwest of the central LHVP site (48.71°N, 2.21°E). A custom built hygroscopic

©2014. American Geophysical Union. All Rights Reserved.

tandem differential mobility analyzer (HTDMA) was used to measure hygroscopic growth factors (GF) at a relative humidity (RH) of 90% for six different dry mobility diameters (35, 50, 75, 110, 165, and 265 nm, d_m). The instrument is described in detail elsewhere [*Tritscher et al*., 2011; *Jurányi et al*., 2013; *Laborde et al*., 2013]. Briefly, aerosol is dried to RH $<$ 15% using a diffusion drier and particles are size selected using the first differential mobility analyzer (DMA). The monodisperse dried particles are then humidified at the target RH (90% in this case) and the number-size distributions of the hydrated particles are determined using a second DMA and a condensation particle counter (TSI model 3022). These size distributions can be expressed as a growth factor (ratio between the wet and dry particle diameter) probability density function (GF-PDF), which describes the likelihood that a particle with a defined dry size exhibits a certain GF at the specified RH [*Gysel et al*., 2009; *Jurányi et al*., 2013]. The TMAinv inversion algorithm was applied to the raw data as described previously [*Gysel et al*., 2009]. The sizing accuracy of the DMAs was periodically checked using polystyrene latex spheres with diameters between 100 and 350 nm. The small sizing difference between the two DMAs (typically less than 1%) was measured and corrected for by switching off the humidification and performing dry measurements of ambient aerosol. The accuracy of the relative humidity measurement was performed using pure ammonium sulphate aerosol as described previously [*Gysel et al*., 2002]. Theoretical hygroscopic growth factor values for the ammonium sulphate calibration were obtained from the Aerosol Diameter Dependent Equilibrium Model [*Topping et al*., 2005]. Both DMAs were placed in a temperature-controlled (20°C) insulated housing, and the relative humidity was measured by a dew point mirror. More details on the humidity and temperature control can be found elsewhere [*Tritscher et al*., 2011]. The HTDMA instrument meets European Supersites for Atmospheric Aerosol Research recommendations [*Massling et al*., 2011]. While a potential artifact associated with evaporation of ammonium nitrate cannot be ruled out, the agreement observed previously between the HTDMA and simultaneous cloud condensation nuclei counter measurements at the SIRTA site [*Jurányi et al*., 2013] suggests that this effect is minimal. Ambient aerosol was sampled through a PM_{10} inlet. Single particle soot photometer (SP2) measurements were also performed at this site for the same period as discussed in detail elsewhere [*Laborde et al*., 2013].

2.2. ATOFMS Data Analysis

ATOFMS mass spectral data were imported using the open-source software package "Enchilada" for further analysis [*Gross et al*., 2010]. Relative sensitivity factors (RSF) for BC, OA, ammonium, nitrate, and sulphate were determined by directly relating the relative peak area (absolute area at a specific *m/z* expressed as a fraction of the total area) of chosen marker ions in the average ATOFMS mass spectrum, detected for each hour of the campaign, to the corresponding mass concentrations measured simultaneously by the HR-ToF-AMS and MAAP instruments. The RSF values, the marker ions used, and the associated assumptions and uncertainties involved in the ATOFMS analysis have been described in detail previously [*Healy et al*., 2013, 2014]. This approach enables estimation of the mass fraction of each chemical species present in each single particle. The five chosen species have been shown to account for more than 90% of the mass of particulate matter smaller than 2.5 μm ($PM_{2.5}$) in Paris [*Bressi et al*., 2013]. Quantification of sodium and chloride, relevant for the hygroscopic growth of marine aerosol, was investigated previously but the ATOFMS mass reconstructions did not agree well with the bulk measurements [*Healy et al*., 2013]. The contribution of sea salt to the sizes investigated here ($<$300 nm) is minimal, although the introduction of single particle estimates of sea salt and crustal composition in future studies would be useful for assessing ice nucleation activity for coarse particles, for example. In this work, in order to estimate the volume fraction of each species at the single particle level, assumed density values were used for BC, OA, and the inorganic ions. Knowledge of the volume fraction and hygroscopic growth factor of each chemical species can thus be used to predict the hygroscopic growth factors of single particles according to the ZSR mixing rule:

$$g_{\mathrm{mix}} \approx \left(\sum_{i}^{N} \varepsilon_i {g_i}^3 \right)^{\frac{1}{3}}, \tag{1}$$

where g_{mix} is the growth factor of the single particle, N is the number of species in the particle, g_i is the growth factor of species i, and ε_i is the volume fraction of species i [*Zdanovskii*, 1948; *Stokes and Robinson*, 1966; *Gysel et al*., 2007; *Duplissy et al*., 2011; *Zamora and Jacobson*, 2013]. Ammonium, sulphate, and nitrate mass fractions were summed to produce a single total "inorganic aerosol" mass fraction value for each single particle. Relative to the high uncertainty associated with single particle mass fraction estimates (40–70%) [*Healy et al*., 2014], small differences in density and hygroscopicity between ammonium nitrate and

©2014. American Geophysical Union. All Rights Reserved.

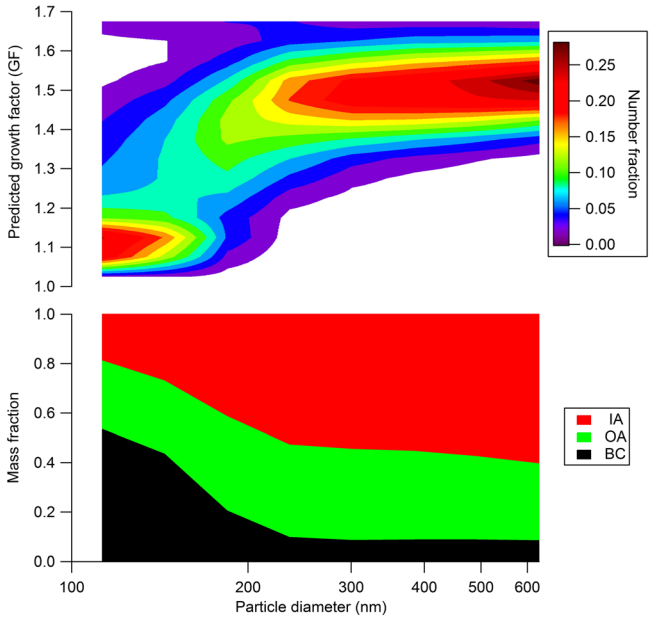

Figure 1. (top) Average dependence of ATOFMS particle counts upon predicted hygroscopic growth factor (at 90% relative humidity) and estimated mobility diameter for the entire measurement period. Particle counts have been normalized in each size bin for clarity. (bottom) Average ATOFMS-derived single particle chemical composition estimates expressed as a function of diameter. IA, OA, and BC refer to inorganic aerosol, organic aerosol, and black carbon, respectively.

ammonium sulphate (<3%) are not expected to contribute significantly to the uncertainty in the total single particle predicted hygroscopicity [*Meyer et al.*, 2009; *Kamilli et al.*, 2014]. All single particle GF calculations were performed for RH = 90% to enable direct comparison with the HTDMA data collected at the SIRTA site.

The oxygen-to-carbon (O/C) ratio of OA has been demonstrated to have an impact upon its hygroscopicity [*Rickards et al.*, 2013], with higher O/C ratios associated with higher hygroscopic growth for OA [*Chang et al.*, 2010; *Duplissy et al.*, 2011; *Tritscher et al.*, 2011]. Hourly GF values for OA were thus calculated using the HR-ToF-AMS data based on previously derived relationships between *f*44 (the relative abundance of the ion signal at *m/z* 44 expressed as a fraction of the total organic signal) and OA hygroscopicity [*Chang et al.*, 2010; *Duplissy et al.*, 2011]. Using the relationships derived in *Chang et al.* [2010] and *Duplissy et al.* [2011], the campaign-averaged GF for bulk OA measured by the HR-ToF-AMS was determined to be 1.19 and 1.21 at 90% RH, respectively. Neither approach led to significantly different results for single particle hygroscopicity as a function of time. Thus, a single constant GF value of 1.2 was used for OA for the entire measurement period.

Density values of 1.77, 1.4, and 2.0 g cm^{-3} and GF values (at RH = 90%) of 1.66, 1.2, and 1.0 were therefore selected for inorganic aerosol, OA, and BC, respectively, based on previous studies [*Gysel et al.*, 2004; *Gysel et al.*, 2007; *Meyer et al.*, 2009; *Liu et al.*, 2013; *Kamilli et al.*, 2014].

3. Results and Discussion

3.1. ATOFMS-Derived Hygroscopic Growth Factors

Hygroscopic growth factors were calculated for all single particles detected by the ATOFMS during the 4 week sampling period (approximately 1.75 million particles). Particles were subsequently binned according to diameter, as discussed elsewhere [*Healy et al.*, 2012], and the size dependence of predicted hygroscopic growth was investigated. ATOFMS aerodynamic diameters have been converted to estimated mobility diameters to enable comparison with the HTDMA measurements. Assuming that all particles are spherical with no internal voids, vacuum aerodynamic diameter and mobility diameter can be related through particle density [*DeCarlo et al.*, 2004; *Slowik et al.*, 2004], an approach that has been previously used to relate size-resolved aerosol mass spectrometer (AMS) composition data with simultaneous HTDMA measurements [*Gysel et al.*, 2007]. The average density of submicron aerosol detected at the LHVP site was previously determined to be 1.5 g cm^{-3} [*Healy et al.*, 2012].

The campaign-averaged dependence of particle number concentration upon the predicted GF (at 90% RH) and particle diameter is shown in Figure 1 (top), together with the average single particle relative composition expressed as a function of diameter (Figure 1 (bottom)). A continuum of single particle GF values is apparent, but two distinct GF modes dominate the distribution. At smaller sizes (≈110 nm), particles have higher BC and OA content, and therefore low GF values (≈1.1). These particles are associated predominantly with traffic and biomass burning sources in the greater Paris area [*Healy et al.*, 2012, 2013; *Laborde et al.*, 2013].

©2014. American Geophysical Union. All Rights Reserved.

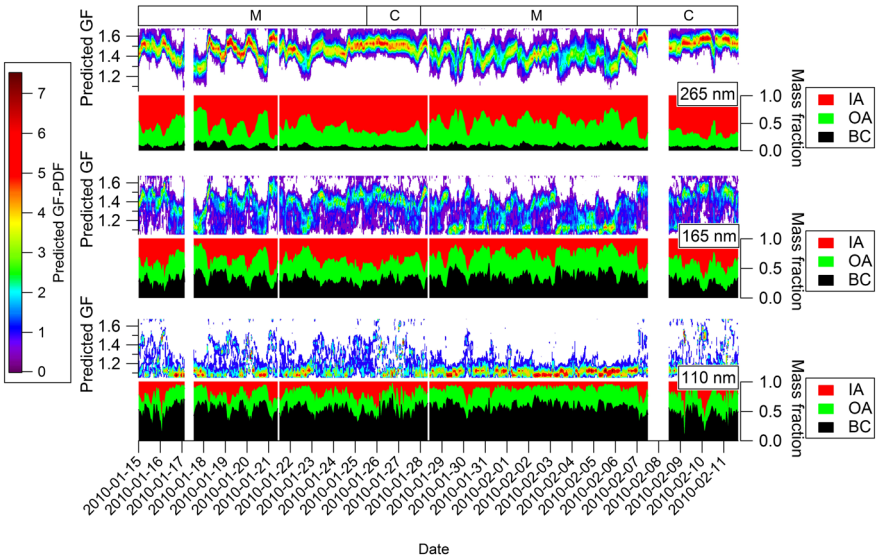

Figure 2. ATOFMS-predicted growth factor probability density functions (GF-PDF) and estimated average chemical composition for single particles of different sizes. "M" and "C" correspond to the periods influenced by marine and continental air masses, respectively.

Larger aged or transported particles (>250 nm) are characterized by higher inorganic ion content, resulting in higher GF values (≈1.5). It is apparent that separate GF modes are not observed at larger diameters, with external mixing only apparent for particles in the size range 150–200 nm, as discussed below. For each size bin, hourly mean predicted GF values were observed to be strongly dependent upon the average mass fraction of inorganic aerosol present. The dependence of hygroscopic growth upon the estimated mass fraction of inorganic aerosol present is expected, due to the higher species GF applied for inorganic aerosol relative to BC and OA, and the cubic relationship in equation (1) [*Gysel et al*., 2004]. The size-resolved ATOFMS-derived estimated mass fractions for nonrefractory species have been previously demonstrated to be in good agreement with simultaneous HR-ToF-AMS measurements [*Healy et al*., 2013]. The association of smaller, less hygroscopic, thinly coated BC particles with local emissions, and larger, more hygroscopic particles containing little or no BC with aged/transported emissions for the greater Paris area is also in agreement with previous SP2 measurements performed during the same measurement period [*Laborde et al*., 2013].

Three ATOFMS size bins, with midpoints at 110, 165, and 265 nm were chosen for further investigation to allow direct comparison with the HTDMA data. The size bins cover a range of ±20 nm in order to contain enough single particles to produce GF distributions, namely 28,866, 64,204, and 232,711 particles for the 110, 165 and 265 nm bins, respectively. Plotting the distribution of predicted GF values for particles of a given diameter as a function of time reflects changes in chemical composition. This GF-PDF is analogous to that produced using traditional HTDMA measurements. If the particle population in a particular size bin were fully internally mixed, a single narrow mode would be observed in the GF-PDF at any given time. If externally mixed aerosol were present, broad or multimodal GF distributions would be observed due to differences in composition for particles of similar size. As shown in Figure 2, for the 110 and 265 nm size bins (top and bottom), relatively narrow unimodal distributions of GF values are predominantly observed, indicating that particles in these size ranges are mostly internally mixed at all times. Smaller GF values are observed for 110 nm particles, consistent with locally emitted combustion particles with low inorganic ion content. Much higher GF values are observed for 265 nm particles, consistent with larger accumulation mode particles that have been subject to atmospheric processing, and thus contain higher inorganic ion content. In contrast, 165 nm particles appear to be externally mixed at times (Figure 2 (middle)), suggesting that particles with low and high inorganic ion content are observed simultaneously at times in this size range.

The influence of air mass origin, assessed using FLEXible PARTicle dispersion model (FLEXPART) model retroplumes [*Stohl et al*., 2005; *Healy et al*., 2012], upon single particle mixing state and hygroscopicity is also apparent in Figure 2. Hygroscopicity for 110 nm particles is relatively unaffected by air mass origin, consistent with fresh, locally

©2014. American Geophysical Union. All Rights Reserved.

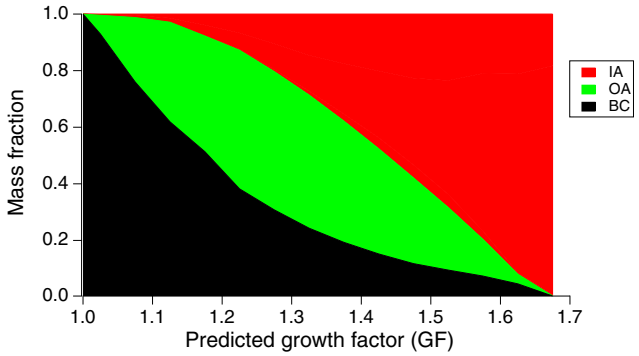

Figure 3. Average composition of 165 ± 20 nm single particles expressed as a function of predicted GF at 90% RH. All particles ($N = 64{,}204$) were first binned according to their predicted GF (bin width = 0.1) and the average composition of each bin was then calculated.

emitted combustion-related carbonaceous particles dominating the particle population in this size range (Figure 2 (bottom)). Different behavior is observed for larger particles, however. During the period influenced most by marine air masses (28 January 00:00 to 07 February 00:00), the 165 nm particle GF-PDF distribution (Figure 2 (middle)) appears to be externally mixed, exhibiting two distinct GF modes at times. This observation suggests that both fresh carbonaceous particles and more aged background particles with higher inorganic ion content are observed simultaneously, and at similar number concentrations under these conditions. In contrast, during continental periods, the relative contribution of locally emitted particles is very low relative to the significantly higher number of particles with high GF values (≈1.5) advected from outside the city, which tend to dominate the GF-PDF. The highest mean GF values for 165 nm particles are observed consistently during periods when the site was influenced by continental air masses, and inorganic ion content was highest. The same trend is apparent for the larger 265 nm particles (Figure 2 (top)).

The value of the ATOFMS-predicted hygroscopicity approach lies in the associated chemical mixing state information. If particles of a given diameter exhibit different chemical composition (external mixing), multiple hygroscopic growth modes will be predicted. As shown in Figure 3, for 165 ± 20 nm particles, those particles with GF values ≤1.1 are on average estimated to be composed almost entirely of BC, with thin OA coatings. As GF increases from 1.1 to 1.2, the mass fraction of BC present in the average single particle decreases significantly from 80% to 40%, and the majority of the coating material at GF = 1.2 is OA. These observations are consistent with coupled HTDMA-SP2 measurements performed at the SIRTA site, where BC particles with GF values ≤1.1 were found to have little or no coating material and were associated predominantly with traffic, while BC particles with GF = 1.2 were proposed to contain a significant fraction of OA and were associated with biomass burning emissions [*Laborde et al*., 2013]. *Laborde et al*. [2013] also observed that for increasing GF values >1.2, BC particle coating thickness remained relatively constant, indicating that increasing GF in the range 1.2–1.6 is controlled by an increase in the ratio of inorganic aerosol to OA present in the BC coating material. This is supported by the ATOFMS composition data for 165 nm particles shown here, which are characterized by a shift from OA-dominated coatings to inorganic ion-dominated coatings as GF increases from 1.2 to 1.6 (Figure 3). These coatings are acquired either through coagulation with preexisting aerosol or by condensation of secondary inorganic and organic aerosol components on BC particles. While the data shown in Figure 3 refers to all particles detected by the ATOFMS in that size range, not exclusively BC-containing particles, both aged BC particles and BC-free particles detected by the HTDMA-SP2 were found to exhibit similar hygroscopic behavior [*Laborde et al*., 2013].

The nature of the chemical differences between particles that exhibit lower and higher predicted GF values can be explored further by querying the ATOFMS mass spectral data set directly. Average dual ion mass spectra for 165 nm particles with GF < 1.2 and 165 nm particles with GF > 1.2 are shown in Figure 4, together with a difference mass spectrum. Examination of this spectrum reveals which chemical species are enhanced in particles with higher predicted GF values. Peaks associated with refractory BC ($[C_n]^-$, $[C_n]^+$) are present both for particles with GF < 1.2 and for particles with GF > 1.2. Higher GF particles exhibit additional peaks representing secondary ammonium $[NH_4]^+$, sulphate $[HSO_4]^-$, and nitrate $[NO_3]^-$. *Liu et al*. [2013] also determined that both secondary ammonium sulphate and nitrate were involved in the atmospheric processing of 163 nm BC particles detected at a coastal site in the UK. In that case, the presence of internally mixed OA was found to suppress the average GF of coated BC particles to values below those expected for pure inorganics (~1.66), an effect that is observed in this work for the 165 nm particles detected in Paris (Figure 2 (middle) and Figure 3).

Furthermore, it is also apparent that during clean marine conditions (28 January 00:00 to 07 February 00:00) (Figure 2 (middle)), relatively small changes in the average bulk inorganic ion mass fraction at a given

©2014. American Geophysical Union. All Rights Reserved.

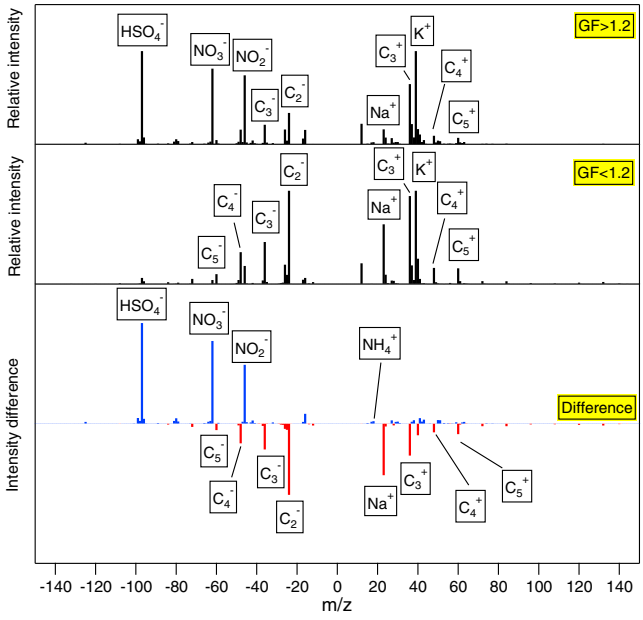

Figure 4. Average mass spectrum of 165 ± 20 nm particles with (top) predicted GF > 1.2, (middle) predicted GF < 1.2, and (bottom) the corresponding difference mass spectrum. Blue peaks represent those species that are present in higher abundance in particles with predicted GF values > 1.2.

diameter may actually arise from significant changes in how externally mixed the particle population is. This has a minor impact on the mean GF value, but a major impact on the associated GF-PDF. ZSR-based bulk aerosol hygroscopicity predictions, for example, provide mean GF values only and do not enable the detection of separate GF modes, instead treating the ensemble as a perfect internal mixture. Knowledge of the number fraction of particles of a given diameter that have high and low inorganic ion mass fractions, provided by single particle mass spectrometers, will thus be useful for modeling efforts aimed at constraining cloud condensation nuclei activity and hygroscopicity [*McMeeking et al*., 2011; *Fierce et al*., 2013].

3.2. Comparison of ATOFMS-Derived and HTDMA Hygroscopic Growth Factors

ATOFMS and HTDMA measurements were performed simultaneously but at separate sites situated 20 km apart. The bulk aerosol composition is on average highly similar between the two sites as discussed in detail in the supporting information and shown in Figures S1–S13. Although the relative contributions of local sources at the LHVP and SIRTA sites are known to differ temporally, a comparison between the ATOFMS-derived predicted growth factors and the HTDMA-measured growth factors was undertaken. The distribution of hourly predicted and hourly measured mean GF values for each particle size investigated is shown in Figure 5. The distribution of predicted GF values and measured GF values is in reasonable agreement for each size investigated, despite the uncertainties associated with both ATOFMS composition estimates and HTDMA GF measurements, and the fact that the measurements took place at separate sites. The mean predicted and measured GF values for 110, 165, and 265 nm particles agree within 6%, 2%, and 1%, respectively.

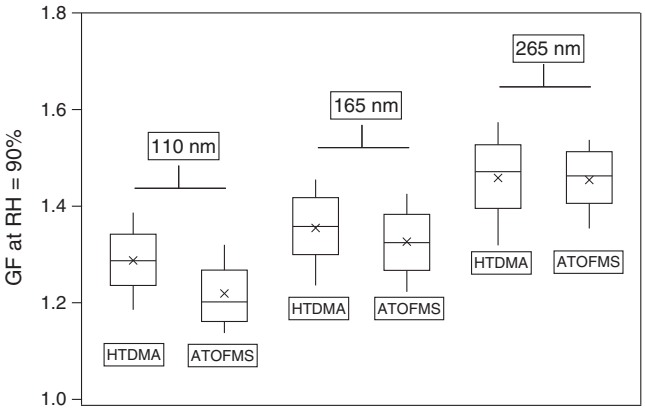

Figure 5. Comparison of HTDMA-measured growth factors at the SIRTA site and ATOFMS-predicted growth factors at the LHVP site for particles of different sizes for each hour of the measurement period ($N = 517$ h). Horizontal lines, boxes, and whiskers represent the median, 75th and 90th percentile values, respectively. The cross markers represent mean values.

The difference in mean ATOFMS-predicted GF values for 110, 165, and 265 nm diameter was found to be statistically significant ($p < 0.01$, unpaired t test), indicating that differences in composition between sizes is controlling the different GF distributions predicted using the ZSR approach. A comparison of GF values predicted in the traditional manner from bulk aerosol composition at the LHVP and SIRTA sites is also included in the supporting information for comparison with the ATOFMS approach (Figures S14–S16). Note that the sample size is smaller for all comparisons in the supporting information because only those periods

©2014. American Geophysical Union. All Rights Reserved.

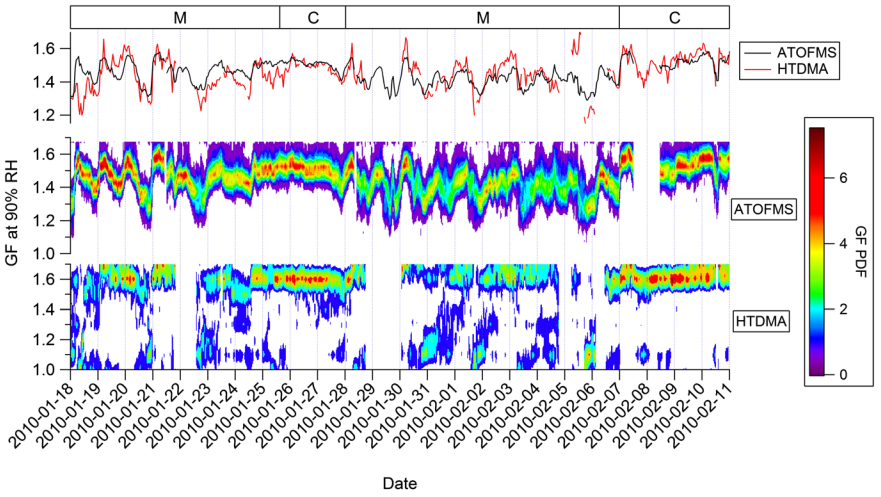

Figure 6. (top) Temporal trends for ATOFMS mean predicted GF values and measured HTDMA mean GF values for 265 ± 20 nm particles. (middle) ATOFMS-predicted growth factor probability density function for 265 ± 20 nm particles. (bottom) HTDMA-measured growth factor probability density function for 265 ± 20 nm particles. M and C correspond to the periods influenced by marine and continental air masses, respectively.

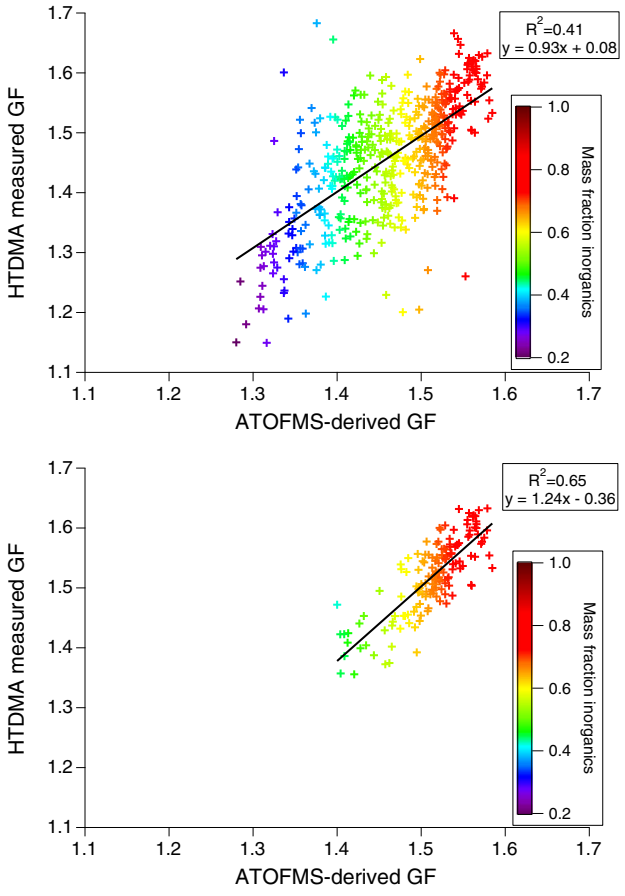

Figure 7. (top) Comparison of ATOFMS mean predicted GF values and measured HTDMA mean GF values for 265 ± 20 nm particles for each hour of the entire measurement period ($N = 517$ h), colored as a function of inorganic aerosol content. (bottom) The same comparison but for periods influenced by continental transport only ($N = 175$ h).

when all instruments at both sites were operating simultaneously are considered ($N = 496$ h). While the bulk aerosol composition GF predictions perform equally as well as ATOFMS GF predictions for 265 nm particles, the mean predicted values for 110 and 165 nm particles are 7–14% higher than the mean measured values. Mean ATOFMS-predicted GF values for 110 and 165 nm, on the other hand, agree within 6% and 2%, respectively, with the measured mean values, because size-resolved composition and mixing state are accounted for. No obvious impact on the relationship between predicted and measured GF values at the SIRTA site as a function of nitrate content is observed, indicating that evaporation of ammonium nitrate in the HTDMA is not significantly influencing the measurements (Figure S17).

Although the distributions of ATOFMS-predicted and HTDMA-measured mean GF values are in good agreement, relatively poor agreement was observed between the temporal patterns of ATOFMS-predicted and HTDMA-measured mean GF values for 110 and 165 nm particles ($R^2 = 0.08$ and 0.20, respectively), although this is not unexpected considering differences in temporality for primary emissions

©2014. American Geophysical Union. All Rights Reserved.

between sites [*Crippa et al*., 2013]. In contrast, the temporal agreement between predicted and measured hygroscopic growth for 265 nm particles was reasonable, as shown for both mean GF values and GF-PDF modes in Figure 6, although some deviations remain apparent ($R^2 = 0.41$). In particular, 265 nm particles with very low GF values are not observed in the ATOFMS GF-PDF, either due to differences in vehicle emission source strength between the sites, or due to uncertainty introduced when assuming a single density value to convert d_{va} to d_m. While ATOFMS-derived and measured hourly mean GF values for 265 nm particles are in reasonable agreement when the entire measurement period is considered (Figure 7 (top)), this agreement improves considerably when only those periods when the city was influenced by continental air masses are considered (25 January 12:00 to 28 January 00:00 and 07 February 00:00 to 11 February 18:00) ($R^2 = 0.65$, Figure 7 (bottom)). This finding is sensible due to the fact that both sites were impacted simultaneously during these periods by aerosol of similar composition advected from outside Paris. As also shown in Figure 7, the highest GF mean values, both predicted and measured, are observed when the average single particle inorganic aerosol mass fraction is highest.

4. Conclusions

Single particle mass spectrometer composition estimates have been used for the first time to predict single particle hygroscopicity using a data set collected in Paris, France, during the MEGAPOLI winter campaign. The Zdanovskii-Stokes-Robinson (ZSR) approach was applied to predict hygroscopic growth based on ATOFMS-derived estimates of OA, inorganic aerosol, and BC content. Small, locally emitted BC particles with low inorganic ion content were predicted to exhibit low hygroscopic growth factors (GF ≈ 1.1 at RH = 90%). Larger, internally mixed particles with higher sulphate and nitrate content, associated with continental transport events, were predicted to have much higher growth factors (GF ≈ 1.5). Mean predicted hygroscopic growth factors for 110, 165, and 265 nm particles were found to agree well with HTDMA mean hygroscopic growth factor data collected at a separate site located 20 km away.

Single particle ZSR hygroscopic growth estimates offer an advantage over routine bulk aerosol ZSR estimates by providing simultaneous chemical composition and mixing state information, thus enabling the prediction of growth factor distributions for particles of a given diameter. Differences in the relative volume fractions of OA and inorganic aerosol present in coatings on BC particles, for example, can be assessed for single particles using this approach. This methodology can be applied to other locations where simultaneous single particle mass spectral data, high temporal resolution bulk composition, and number-size distribution data are available. Codeployment of a soot particle aerosol mass spectrometer would also enable higher accuracy quantitative single particle speciation by providing size-resolved bulk composition for BC, OA, and inorganic ions. Quantitative single particle chemical composition will be useful for improving and validating climate models that can incorporate aerosol mixing state, in particular for environments where external mixing is relevant.

Acknowledgments

The authors wish to thank Monica Crippa for providing AMS mass concentration data for the SIRTA site. This work has been funded by the Marie Curie Action FP7-PEOPLE-IOF-2011 (Project: CHEMBC, 299755) and the EU Seventh Framework Programme FP/2007-2011 (MEGAPOLI). M.G. received financial support from ERC-2013-CoG 615922-BLACARAT. All data used for the preparation of this manuscript are freely available on request through the corresponding author.

References

Allen, J. O., P. V. Bhave, J. R. Whiteaker, and K. A. Prather (2006), Instrument busy time and mass measurement using aerosol time-of-flight mass spectrometry, *Aerosol Sci. Technol.*, *40*(8), 615–626.

Bauer, S. E., A. Ault, and K. A. Prather (2013), Evaluation of aerosol mixing state classes in the GISS modelE-MATRIX climate model using single-particle mass spectrometry measurements, *J. Geophys. Res. Atmos.*, *118*, 9834–9844, doi:10.1002/jgrd.50700.

Bressi, M., J. Sciare, V. Ghersi, N. Bonnaire, J. B. Nicolas, J. E. Petit, S. Moukhtar, A. Rosso, N. Mihalopoulos, and A. Féron (2013), A one-year comprehensive chemical characterisation of fine aerosol ($PM_{2.5}$) at urban, suburban and rural background sites in the region of Paris (France), *Atmos. Chem. Phys.*, *13*(15), 7825–7844.

Buzorius, G., A. Zelenyuk, F. Brechtel, and D. Imre (2002), Simultaneous determination of individual ambient particle size, hygroscopicity and composition, *Geophys. Res. Lett.*, *29*(20), 1974, doi:10.1029/2001GL014221.

Chang, R. Y. W., J. G. Slowik, N. C. Shantz, A. Vlasenko, J. Liggio, S. J. Sjostedt, W. R. Leaitch, and J. P. D. Abbatt (2010), The hygroscopicity parameter (κ) of ambient organic aerosol at a field site subject to biogenic and anthropogenic influences: Relationship to degree of aerosol oxidation, *Atmos. Chem. Phys.*, *10*(11), 5047–5064.

Corbin, J. C., P. J. G. Rehbein, G. J. Evans, and J. P. D. Abbatt (2012), Combustion particles as ice nuclei in an urban environment: Evidence from single-particle mass spectrometry, *Atmos. Environ.*, *51*(0), 286–292.

Crippa, M., et al. (2013), Wintertime aerosol chemical composition and source apportionment of the organic fraction in the metropolitan area of Paris, *Atmos. Chem. Phys.*, *13*(2), 961–981.

Cziczo, D. J., D. S. Thomson, T. L. Thompson, P. J. DeMott, and D. M. Murphy (2006), Particle analysis by laser mass spectrometry (PALMS) studies of ice nuclei and other low number density particles, *Int. J. Mass Spectrom.*, *258*(1–3), 21–29.

Cziczo, D. J., K. D. Froyd, C. Hoose, E. J. Jensen, M. H. Diao, M. A. Zondlo, J. B. Smith, C. H. Twohy, and D. M. Murphy (2013), Clarifying the dominant sources and mechanisms of cirrus cloud formation, *Science*, *340*(6138), 1320–1324.

©2014. American Geophysical Union. All Rights Reserved.

DeCarlo, P. F., J. G. Slowik, D. R. Worsnop, P. Davidovits, and J. L. Jimenez (2004), Particle morphology and density characterization by combined mobility and aerodynamic diameter measurements. Part 1: Theory, *Aerosol Sci. Technol.*, *38*, 1185–1205.
DeCarlo, P. F., et al. (2006), Field-deployable, high-resolution, time-of-flight aerosol mass spectrometer, *Anal. Chem.*, *78*(24), 8281–8289.
Duplissy, J., et al. (2011), Relating hygroscopicity and composition of organic aerosol particulate matter, *Atmos. Chem. Phys.*, *11*(3), 1155–1165.
Ferge, T., E. Karg, A. Schröppel, K. R. Coffee, H. J. Tobias, M. Frank, E. E. Gard, and R. Zimmermann (2006), Fast determination of the relative elemental and organic carbon content of aerosol samples by on-line single-particle aerosol time-of-flight mass spectrometry, *Environ. Sci. Technol.*, *40*(10), 3327–3335.
Fierce, L., N. Riemer, and T. C. Bond (2013), When is cloud condensation nuclei activity sensitive to particle characteristics at emission?, *J. Geophys. Res. Atmos.*, *118*, 13,476–413,488, doi:10.1002/2013JD020608.
Froyd, K. D., S. M. Murphy, D. M. Murphy, J. A. de Gouw, N. C. Eddingsaas, and P. O. Wennberg (2010), Contribution of isoprene-derived organosulfates to free tropospheric aerosol mass, *Proc. Natl. Acad. Sci. U.S.A.*, *107*(50), 21,360–21,365.
Gard, E., J. E. Mayer, B. D. Morrical, T. Dienes, D. P. Fergenson, and K. A. Prather (1997), Real-time analysis of individual atmospheric aerosol particles: Design and performance of a portable ATOFMS, *Anal. Chem.*, *69*(20), 4083–4091.
Gross, D. S., et al. (2010), Environmental chemistry through intelligent atmospheric data analysis, *Environ. Modell. Software*, *25*, 760–769.
Gysel, M., E. Weingartner, and U. Baltensperger (2002), Hygroscopicity of aerosol particles at low temperatures. 2. Theoretical and experimental hygroscopic properties of laboratory generated aerosols, *Environ. Sci. Technol.*, *36*(1), 63–68.
Gysel, M., E. Weingartner, S. Nyeki, D. Paulsen, U. Baltensperger, I. Galambos, and G. Kiss (2004), Hygroscopic properties of water-soluble matter and humic-like organics in atmospheric fine aerosol, *Atmos. Chem. Phys.*, *4*(1), 35–50.
Gysel, M., J. Crosier, D. O. Topping, J. D. Whitehead, K. N. Bower, M. J. Cubison, P. Williams, M. Flynn, G. McFiggans, and H. Coe (2007), Closure between chemical composition and hygroscopic growth of aerosol particles during TORCH2, in *Nucleation and Atmospheric Aerosols*, edited by C. O'Dowd and P. Wagner, pp. 731–735, Springer, Netherlands, doi:10.1007/978-1-4020-6475-3_144.
Gysel, M., G. B. McFiggans, and H. Coe (2009), Inversion of tandem differential mobility analyser (TDMA) measurements, *J. Aerosol Sci.*, *40*(2), 134–151.
Healy, R. M., et al. (2012), Sources and mixing state of size-resolved elemental carbon particles in a European megacity: Paris, *Atmos. Chem. Phys.*, *12*(4), 1681–1700.
Healy, R. M., et al. (2013), Quantitative determination of carbonaceous particle mixing state in Paris using single-particle mass spectrometer and aerosol mass spectrometer measurements, *Atmos. Chem. Phys.*, *13*(18), 9479–9496.
Healy, R. M., et al. (2014), Single particle diversity and mixing state measurements, *Atmos. Chem. Phys.*, *14*, 6289–6299.
Hegg, D. A., D. S. Covert, and H. H. Jonsson (2008), Measurements of size-resolved hygroscopicity in the California coastal zone, *Atmos. Chem. Phys.*, *8*(23), 7193–7203.
Herich, H., L. Kammermann, M. Gysel, E. Weingartner, U. Baltensperger, U. Lohmann, and D. J. Cziczo (2008), In situ determination of atmospheric aerosol composition as a function of hygroscopic growth, *J. Geophys. Res.*, *113*, D16213, doi:10.1029/2008JD009954.
Herich, H., L. Kammermann, B. Friedman, D. S. Gross, E. Weingartner, U. Lohmann, P. Spichtinger, M. Gysel, U. Baltensperger, and D. J. Cziczo (2009), Subarctic atmospheric aerosol composition: 2. Hygroscopic growth properties, *J. Geophys. Res.*, *114*, D13204, doi:10.1029/2008JD011574.
Hersey, S. P., A. Sorooshian, S. M. Murphy, R. C. Flagan, and J. H. Seinfeld (2009), Aerosol hygroscopicity in the marine atmosphere: A closure study using high-time-resolution, multiple-RH DASH-SP and size-resolved C-ToF-AMS data, *Atmos. Chem. Phys.*, *9*(7), 2543–2554.
Hersey, S. P., et al. (2013), Composition and hygroscopicity of the Los Angeles Aerosol: CalNex, *J. Geophys. Res. Atmos.*, *118*, 3016–3036, doi:10.1002/jgrd.50307.
Jeong, C. H., M. L. McGuire, K. J. Godri, J. G. Slowik, P. J. G. Rehbein, and G. J. Evans (2011), Quantification of aerosol chemical composition using continuous single particle measurements, *Atmos. Chem. Phys.*, *11*(14), 7027–7044.
Jurányi, Z., T. Tritscher, M. Gysel, M. Laborde, L. Gomes, G. Roberts, U. Baltensperger, and E. Weingartner (2013), Hygroscopic mixing state of urban aerosol derived from size-resolved cloud condensation nuclei measurements during the MEGAPOLI campaign in Paris, *Atmos. Chem. Phys.*, *13*(13), 6431–6446.
Kamilli, K. A., L. Poulain, A. Held, A. Nowak, W. Birmili, and A. Wiedensohler (2014), Hygroscopic properties of the Paris urban aerosol in relation to its chemical composition, *Atmos. Chem. Phys.*, *14*(2), 737–749.
Laborde, M., et al. (2013), Black carbon physical properties and mixing state in the European megacity Paris, *Atmos. Chem. Phys.*, *13*(11), 5831–5856.
Levin, E. J. T., A. J. Prenni, B. B. Palm, D. A. Day, P. Campuzano-Jost, P. M. Winkler, S. M. Kreidenweis, P. J. DeMott, J. L. Jimenez, and J. N. Smith (2014), Size-resolved aerosol composition and its link to hygroscopicity at a forested site in Colorado, *Atmos. Chem. Phys.*, *14*(5), 2657–2667.
Liu, D., J. Allan, J. Whitehead, D. Young, M. Flynn, H. Coe, G. McFiggans, Z. L. Fleming, and B. Bandy (2013), Ambient black carbon particle hygroscopic properties controlled by mixing state and composition, *Atmos. Chem. Phys.*, *13*(4), 2015–2029.
Massling, A., et al. (2011), Results and recommendations from an intercomparison of six Hygroscopicity-TDMA systems, *Atmos. Meas. Tech.*, *4*(3), 485–497.
McMeeking, G. R., N. Good, M. D. Petters, G. McFiggans, and H. Coe (2011), Influences on the fraction of hydrophobic and hydrophilic black carbon in the atmosphere, *Atmos. Chem. Phys.*, *11*(10), 5099–5112.
Meyer, N. K., et al. (2009), Analysis of the hygroscopic and volatile properties of ammonium sulphate seeded and unseeded SOA particles, *Atmos. Chem. Phys.*, *9*(2), 721–732.
Neubauer, K. R., M. V. Johnston, and A. S. Wexler (1998), Humidity effects on the mass spectra of single aerosol particles, *Atmos. Environ.*, *32*(14–15), 2521–2529.
Petzold, A., and M. Schönlinner (2004), Multi-angle absorption photometry—A new method for the measurement of aerosol light absorption and atmospheric black carbon, *J. Aerosol Sci.*, *35*(4), 421–441.
Pratt, K. A., L. E. Hatch, and K. A. Prather (2009), Seasonal volatility dependence of ambient particle phase amines, *Environ. Sci. Technol.*, *43*(14), 5276–5281.
Qin, X., P. V. Bhave, and K. A. Prather (2006), Comparison of two methods for obtaining quantitative mass concentrations from aerosol time-of-flight mass spectrometry measurements, *Anal. Chem.*, *78*(17), 6169–6178.
Rickards, A. M. J., R. E. H. Miles, J. F. Davies, F. H. Marshall, and J. P. Reid (2013), Measurements of the sensitivity of aerosol hygroscopicity and the κ parameter to the O/C ratio, *J. Phys. Chem. A*, *117*(51), 14,120–14,131.
Riemer, N., M. West, R. A. Zaveri, and R. C. Easter (2009), Simulating the evolution of soot mixing state with a particle-resolved aerosol model, *J. Geophys. Res.*, *114*, D09202, doi:10.1029/2008JD011073.
Sjogren, S., M. Gysel, E. Weingartner, M. R. Alfarra, J. Duplissy, J. Cozic, J. Crosier, H. Coe, and U. Baltensperger (2008), Hygroscopicity of the submicrometer aerosol at the high-alpine site Jungfraujoch, 3580 m a.s.l., Switzerland, *Atmos. Chem. Phys.*, *8*(18), 5715–5729.
Slowik, J. G., K. Stainken, P. Davidovits, L. R. Williams, J. T. Jayne, C. E. Kolb, D. R. Worsnop, Y. Rudich, P. F. DeCarlo, and J. L. Jimenez (2004), Particle morphology and density characterization by combined mobility and aerodynamic diameter measurements. Part 2: Application to combustion-generated soot aerosols as a function of fuel equivalence ratio, *Aerosol Sci. Technol.*, *38*, 1206–1222.

©2014. American Geophysical Union. All Rights Reserved.

Stohl, A., C. Forster, A. Frank, P. Seibert, and G. Wotawa (2005), Technical note: The Lagrangian particle dispersion model FLEXPART version 6.2, *Atmos. Chem. Phys.*, *5*(9), 2461–2474.

Stokes, R. H., and R. A. Robinson (1966), Interactions in aqueous nonelectrolyte solutions. I. Solute-solvent equilibria, *J. Phys. Chem.*, *70*(7), 2126–2131.

Su, Y., M. F. Sipin, H. Furutani, and K. A. Prather (2004), Development and characterization of an aerosol time-of-flight mass spectrometer with increased detection efficiency, *Anal. Chem.*, *76*(3), 712–719.

Sullivan, R. C., M. J. Moore, M. D. Petters, S. M. Kreidenweis, G. C. Roberts, and K. A. Prather (2009), Timescale for hygroscopic conversion of calcite mineral particles through heterogeneous reaction with nitric acid, *Phys. Chem. Chem. Phys.*, *11*, 7826–7837.

Svenningsson, B., et al. (2006), Hygroscopic growth and critical supersaturations for mixed aerosol particles of inorganic and organic compounds of atmospheric relevance, *Atmos. Chem. Phys.*, *6*(7), 1937–1952.

Topping, D. O., G. B. McFiggans, and H. Coe (2005), A curved multi-component aerosol hygroscopicity model framework: Part 1 – Inorganic compounds, *Atmos. Chem. Phys.*, *5*(5), 1205–1222.

Tritscher, T., et al. (2011), Volatility and hygroscopicity of aging secondary organic aerosol in a smog chamber, *Atmos. Chem. Phys.*, *11*(22), 11,477–11,496.

Tuch, T. M., A. Haudek, T. Müller, A. Nowak, H. Wex, and A. Wiedensohler (2009), Design and performance of an automatic regenerating adsorption aerosol dryer for continuous operation at monitoring sites, *Atmos. Meas. Tech.*, *2*(2), 417–422.

Wu, Z. J., et al. (2013), Relating particle hygroscopicity and CCN activity to chemical composition during the HCCT-2010 field campaign, *Atmos. Chem. Phys. Discuss.*, *13*(3), 7643–7680.

Zamora, I. R., and M. Z. Jacobson (2013), Measuring and modeling the hygroscopic growth of two humic substances in mixed aerosol particles of atmospheric relevance, *Atmos. Chem. Phys.*, *13*(17), 8973–8989.

Zdanovskii, A. (1948), New methods for calculating solubilities of electrolytes in multicomponent systems, *Zh. Fiz. Khim.*, *22*, 1475–1485.

Zelenyuk, A., D. Imre, and L. A. Cuadra-Rodriguez (2006), Evaporation of water from particles in the aerodynamic lens inlet: An experimental study, *Anal. Chem.*, *78*(19), 6942–6947.

Zelenyuk, A., D. Imre, M. Earle, R. Easter, A. Korolev, R. Leaitch, P. Liu, A. M. Macdonald, M. Ovchinnikov, and W. Strapp (2010), In situ characterization of cloud condensation nuclei, interstitial, and background particles using the single particle mass spectrometer, SPLAT II, *Anal. Chem.*, *82*(19), 7943–7951.

©2014. American Geophysical Union. All Rights Reserved.